Energy 138 (2017) 728–738

Contents lists available at ScienceDirect

Energy

journal homepage: www.elsevier.com/locate/energy

Modeling and analysis of short-period transient response of a single, planar, anode supported, solid oxide fuel cell during load variations

Marko Nerat

Jožef Stefan Institute (JSI), Jamova 39, SI–1000 Ljubljana, Slovenia

ARTICLE INFO

Article history:
Received 7 April 2017
Received in revised form
19 June 2017
Accepted 20 July 2017
Available online 24 July 2017

Keywords:
3-D dynamic model
Load variation
Transient response
Fuel starvation
Power density
Conversion efficiency of SOFC

ABSTRACT

The main motivation for this study was to analyze transient responses of a solid oxide fuel cell (SOFC) during load variations, which can possibly cause fuel starvation within porous anode active layer and, consequently, accelerate the degradation rate of the SOFC. Simulation approach was taken into consideration. For this purpose, three-dimensional (3-D) dynamic model of a single, planar, anode supported SOFC was built. The model is also briefly presented in this paper. The paper focuses on detailed transient analysis of current density (J), power density (P), fuel utilization (FU) and electrical conversion efficiency (η) after a step change of voltage (load). The simulation results also give us valuable data about local mass fractions of fuel species that cannot be measured in realistic devices. It is shown that fuel starvation occurs when the J (load) is increased by approximately 100% and FU is above 0.85 at final value of J (when steady state is assumed). Moreover, the time-dependent profile of FU give us guideline for setting appropriate inlet flow rate of fuel to prevent fuel starvation. The results show that a SOFC with very thin ($d_s = 0.1$ mm) porous anode support layer is prone to fuel starvation during large load variation. Using a thicker porous anode support layer ($d_s = 0.5$ mm) is proposed to avoid fuel starvation and, consequently, mitigate the degradation of a realistic SOFC. The P and η of modeled SOFC are also analyzed during large load variations. The η increases with increasing the d_s from 0.1 mm to 1.0 mm. The results indicate the improvement of η by appropriate design and control of a realistic SOFC.

1. Introduction

Fuel cells (FCs) have gained interest lately since they convert chemical energy of the fuel directly into electrical energy with high conversion efficiency [1]. Some FCs must be supplied with pure hydrogen as a fuel, e.g. proton exchange membrane (PEM) FCs, which operate at low temperatures ($T < 100$ °C), whereas the others can be supplied with different mixtures of fuels, with e.g. hydrogen (H_2) and methane (CH_4) [2]. One of potentially successful FCs, which can be supplied with hydro-carbon fuels, are solid oxide fuel cells (SOFCs). They operate at high temperatures ($T = 650–1000$ °C) [3].

In the past years, many efforts have been made to improve reliability of solid oxide fuel cell (SOFC) electric power generators. Experimental studies indicated that degradation processes within the SOFC structures, which commonly consist of stacked PEN, i.e. positive electrode (cathode) - electrolyte (solid oxide) - negative electrode (anode), structures, represent the limitation to the operational lifetime [4–6], and consequently, to the beneficial mass production and commercialization of such systems.

The degradation of SOFC occurs due to different agents, which may be attributed to operational conditions [7], or due to low steam-to-carbon ratio (STCR below 2) [8], that probably causes solid carbon deposition within the porous anode support and active layer. The solid carbon reduces electrochemical activity of triple phase boundaries (TPBs). Beside this, excessive local temperatures or temperature gradients also cause degradation of electrochemical performance [9], or even failure of SOFC over a long term of operation [10].

The anode degradation is one of critical problems which has been extensively investigated by experimental [11] and theoretical studies [12]. The local fuel starvation inside the porous anode layer leads to local anode reoxidation [7] and degradation of the SOFC [13]. The latter situation is likely to occur when the electric load, which is connected to SOFC generator, is abruptly increased. Consequently, the total electric current (or current density) of SOFC is increased (the output voltage is decreased), which means that

E-mail address: marko.nerat@ijs.si.

http://dx.doi.org/10.1016/j.energy.2017.07.133
0360-5442/

more fuel (if available) is used by electrochemical reactions. In particular case, when almost all fuel is locally used, fuel utilization (FU) approaches to one, which may be critical for anode degradation. Cumulatively, such periods of fuel starvation can cause irreversible damage to SOFC [14].

The main problem to achieve appropriate FU is the slowness of fuel flow control (even if feed-forward control is used and the fuel flow is adjusted proportionally with load current), since the blower and/or valve cannot increase (decrease) fuel flow instantly to follow the desired load change. Moreover, there is also some propagation delay of the fuel gases to reach the reaction sites within the porous anode active layer. However, these problems could be mitigated by using current rate limiters [15], but far more sophisticated current-voltage control would be necessary [16].

Many studies have been done to analyze the dynamic response of the SOFC after applying a step variation of load (i.e. current or voltage) [17,18]. Some results show that current (voltage) is subjected to a short-period (about 1 s) overshoot during the transient before it settles at its steady-state value [19]. A sound comparison between the results obtained by different researchers using different models is given in recent publication [20].

However, most models employed in dynamic mode simulation are restricted to one- or two dimensions (1D or 2D) due to reducing the computational demands (time and memory). The selection of SOFC model accuracy thus usually follows model purpose, but it often becomes inappropriate due to a lack of understanding how model simplifications reflect on the final results. The 1-D models are simplified so they lack fuel storage within the porous anode support and active layer. The stored fuel may be important during the transients [20].

It would be of high importance if the current overshoot, which was identified during the load transients [19], could be reduced and, consequently, the local fuel starvation would be reduced. Due to the latter, it could be expected that the degradation process, which is caused by local anode reoxidation, might be slowed down.

This paper presents a transient analysis of current density (J), power density (P), fuel utilization (FU) and conversion efficiency (η) after applied changes of voltage (load), and gives deeper insight into the time-variable mass fractions of fuel species within the porous anode active layer. The simulation results obtained by using our 3-D dynamic model of a single, planar, anode supported SOFC, which has been developed in COMSOL Multiphysics® 4.3 [21], are also compared with results from literature [19,20,22–24].

There are many recently published papers that concentrate on computational fluid dynamics modeling. One of them studies the impact of the fuel flow distribution on the maximum obtainable conversion during operation and the obtainable overall conversion is found to be directly proportional to the flow uniformity [25]. However, dynamic operation of the studied SOFC was not addressed. Another study revealed that molar (or mass) fraction of carbon monoxide (CO) at the anode can be well controlled by adjusting the operating conditions of direct carbon (DC) SOFC. It was also found that anode-supported configuration is beneficial in improving the electrical output of the DC-SOFC, but no data about electrical power, conversion efficiency or molar fraction of CO during load variations can be found in that paper [26]. The latter may be of high importance since molar fractions of fuel species cannot be measured locally in realistic devices. The molar fractions of gases in multi-channel anode-supported planar SOFC have been studied in details by using 3-D model [27], whereas no evidence of their transient response can be found. The electrochemical performance of SOFC during load-following operation was studied in Ref. [28], but only a simplified (0-D) Matlab/Simulink model based on experimental data was used.

2-D dynamic model for hydrogen-fed and methane-fed SOFCs has been presented in Ref. [29]. The current density in start-up procedure and electrical efficiency at different inlet temperature of SOFC were studied. The paper does not provide results about transient response of current density or electrical efficiency during load variations.

The advantage of 3-D dynamic model is that the local concentrations (molar or mass fractions) of fuel species can be monitored and their minimum values can be revealed. The latter is important to identify (possible) local fuel starvation and also to give some guidelines for setting an appropriate fuel utilization (FU) to prevent fuel starvation and to achieve high conversion efficiency. To the best author's knowledge there is some gap in the field of 3-D dynamic modeling and transient response of SOFC during load variations. Most of the studies focus on steady-state analysis [30,31], whereas only a few of them concentrate on transient analysis [32], so this paper is an important step forward in the field of 3-D dynamic modeling and analysis of SOFC operation during load variations. Moreover, no data about the effect of diverse thickness of porous anode support layer (d_s) on the electrochemical performance of a SOFC during the transients has been found. This paper also deals with fuel starvation issues that emerge at SOFC with thin porous anode support layer during large load variations and indicates optimum d_s by means of achieving high electrical conversion efficiency (η).

The main goal of this analysis is to indicate possible solutions to improve η of the SOFC and mitigate the degradation risks concurrently. The presented results are intended for a number of experimentalists to help them design realistic SOFC devices in time-efficient way and at reduced costs. The presented analysis also opens an interesting research area in optimum design of SOFC, since improving the η of SOFC seems increasingly important.

The main novelty of this paper is a detailed study of electrochemical performances of SOFC using 3-D dynamic model, which is mandatory to give us deep insight into operation of SOFC during load variations.

2. Modeling

A three-dimensional (3-D) thermo-fluid model of a single, planar, anode-supported SOFC has been developed in COMSOL Multiphysics® 4.3 and thoroughly presented in our previous paper [21].

However, the main difference between that model and the model used in this study stems from time-dependent physical variables. The software package COMSOL Multiphysics® 4.3 provides quite simple implementation of dynamic model by selecting appropriate option (e.g. time-discrete model).

The equations used in this 3-D dynamic model are summarized in the next sections to show differences compared to steady state model. Interested reader is referred to a detailed description of the steady state model, which is presented in Ref. [21].

2.1. Gas chambers

The flow of gases within the gas chambers is modeled by the following equations:

- Continuity equation

$$\frac{\partial \rho}{\partial t} + \vec{\nabla} \cdot \left(\rho \vec{v}\right) = 0 \tag{1}$$

- Momentum equation:

$$\rho\frac{\partial\vec{v}}{\partial t}+\rho\left(\vec{v}\cdot\vec{\nabla}\right)\vec{v}=\vec{\nabla}\cdot\left[-pI+\mu\left(\left(\vec{\nabla}\ \vec{v}\right)+\left(\vec{\nabla}\ \vec{v}\right)^{\mathrm{T}}\right)-\frac{2\mu}{3}\left(\vec{\nabla}\cdot\vec{v}\right)I\right] \tag{2}$$

- Species conservation equation:

$$\rho\frac{\partial x_{\mathrm{i}}}{\partial t}+\vec{\nabla}\cdot\vec{j}_{\mathrm{i}}+\rho\left(\vec{v}\cdot\vec{\nabla}\right)x_{\mathrm{i}}=0 \tag{3}$$

where ρ is specific density of gas mixture, v is velocity of gases, p is pressure of gases, μ is viscosity of gases, x_{i} is mole fraction of i-th gas specie, and j_{i} is the multicomponent diffusive mass flux. The density ρ is obtained by considering N ideal gas species (i) in the mixture:

$$\rho=\left(\frac{RT}{p}\sum_{\mathrm{i}=1}^{\mathrm{N}}\frac{Y_{\mathrm{i}}}{M_{\mathrm{i}}}\right)^{-1}, \tag{4}$$

where R is standard gas constant, T is gas temperature, Y_{i} is mass fraction and M_{i} is molar mass of i-th gas specie, respectively. Furthermore, x_{i} is calculated from the following equation:

$$x_{\mathrm{i}}=\frac{Y_{\mathrm{i}}}{M_{\mathrm{i}}}\left(\sum_{\mathrm{i}=1}^{\mathrm{N}}x_{\mathrm{i}}M_{\mathrm{i}}\right), \tag{5}$$

j_{i} is the multicomponent diffusive mass flux and is calculated as:

$$\vec{j}_{\mathrm{i}}=-\rho x_{\mathrm{i}}\left(\sum_{\mathrm{j}=1}^{\mathrm{N}}D_{\mathrm{i,j,eff}}\vec{d}_{\mathrm{j}}\right), \tag{6}$$

where $D_{\mathrm{i,j,eff}}$ is effective diffusion coefficient, whereas d_{j} is calculated as follows:

$$\vec{d}_{\mathrm{j}}=\vec{\nabla}\,X_{\mathrm{j}}+\frac{(X_{\mathrm{j}}-x_{\mathrm{j}})\vec{\nabla}\,p}{p} \tag{7}$$

and X_{j} is defined as:

$$X_{\mathrm{j}}=x_{\mathrm{j}}\left(M_{\mathrm{j}}\left(\sum_{\mathrm{i}=1}^{\mathrm{N}}\frac{x_{\mathrm{i}}}{M_{\mathrm{i}}}\right)\right)^{-1} \tag{8}$$

2.2. Porous electrodes

Gas diffusion anode and cathode layers consist of porous media that serve to transport gaseous species to and away from the active reaction sites at the porous electrode/electrolyte interfaces. Beside this, porous electrodes also conduct generated electric current from the reaction sites to the current collectors and contacts of the SOFC. The continuity and momentum equations are implemented to model porous matrix properties:

- Continuity equation

$$\frac{\partial(\varepsilon_{\mathrm{p}}\rho)}{\partial t}+\vec{\nabla}\cdot\left(\rho\vec{v}\right)=Q \tag{9}$$

- Momentum equation:

$$\frac{\rho}{\varepsilon_{\mathrm{p}}}\left(\frac{\partial\vec{v}}{\partial t}+\left(\vec{v}\cdot\vec{\nabla}\right)\frac{\vec{v}}{\varepsilon_{\mathrm{p}}}\right)=\vec{\nabla}\cdot\left[-pI+\frac{\mu}{\varepsilon_{\mathrm{p}}}\left(\left(\vec{\nabla}\ \vec{v}\right)+\left(\vec{\nabla}\ \vec{v}\right)^{\mathrm{T}}\right)-\frac{2\mu}{3\varepsilon_{\mathrm{p}}}\left(\vec{\nabla}\cdot\vec{v}\right)I\right]-\left(\frac{\mu}{\kappa}+Q\right)\vec{v}, \tag{10}$$

where ε_{p} is porosity and κ is permeability of porous electrodes. The porous electrode coupling is considered by summing up the products of reaction rates and molar masses of all involved gas species (i) within the anode or cathode porous layer, by the following equation:

$$Q=\sum_{\mathrm{j}=0}^{\mathrm{N}}\sum_{\mathrm{i}=0}^{\mathrm{N}}R_{\mathrm{i,j}}M_{\mathrm{i}} \tag{11}$$

- Charge conservation equation:

The electronic current transport in porous electrodes is modeled by considering conservation of electric charge in a solid metal conductor:

$$\vec{\nabla}\cdot\left(-\sigma_{\mathrm{s,eff}}\vec{\nabla}\,\varphi_{\mathrm{s}}\right)=0 \tag{12}$$

where $\sigma_{\mathrm{s,eff}}$ is effective electronic conductivity of porous electrode and ϕ_{s} is electrostatic potential in solid phase.

- Energy conservation equation:

The energy transport in porous electrodes is modeled by considering effective thermal conductivity ($k_{\mathrm{s,eff}}$), and effective product of specific heat (C_p) and specific density (ρ) of the solid material:

$$(\rho C_p)_{\text{eff}} \frac{\partial T}{\partial t} = \vec{\nabla} \cdot \left(k_{\text{s,eff}} \vec{\nabla} T \right) + S_{\text{e}}, \quad (13)$$

where S_{e} is heat source and it is considered that heat is generated due to ohmic heat losses within the porous electrodes when electric current flows through:

$$S_{\text{e}} = \vec{J} \cdot \vec{E} = \sigma_{\text{s,eff}} \vec{E} \cdot \vec{E} = \sigma_{\text{s,eff}} \vec{\nabla} \varphi_{\text{s}} \cdot \vec{\nabla} \varphi_{\text{s}} \quad (14)$$

J denotes electric current density and E denotes electrostatic field (i.e. negative gradient of electrostatic potential ϕ_{s}). The values of $\sigma_{\text{s,eff}}$, $k_{\text{s,eff}}$, C_p and ρ can be found in Table 6 in Ref. [21].

2.3. Catalyst layers, electrolyte and contacts

The implemented equations for modeling electronic/ionic current transport and heat generation/exchange in catalyst layers, electrolyte and contacts have been extensively described in our previous paper and are not repeated here. The main difference between the presented energy conservation equations in Ref. [21], and the implemented equations here, is additional term with time derivative of temperature T, as can be seen in (13).

3. Results and discussion

One of the most important aspects at development of SOFC electric generators is reducing the degradation processes to make these devices suitable for long-term efficient operation, as already mentioned in Introduction. Since the experimental tests are usually expensive, time and energy consumptive, it makes sense to build a suitable model of SOFC and to explore possibilities for slowing down the degradation processes and improving the efficiency by means of simulation results.

For this purpose, a numerical study using a 3-D dynamic, thermo-fluid model of a single, planar, anode-supported SOFC has been conducted. First of all, the baseline model was set, similar to input parameters listed in Ref. [21]. For convenience, the reference pressure (p_{ref}), ambient temperature (T_{amb}), velocity of fuel at anode inlet ($v_{\text{in,a}}$), velocity of air at cathode inlet ($v_{\text{in,c}}$), porosity (ε_{p}) and permeability (κ) of support/active layers are listed in Table 1. It is assumed that modeled SOFC operates inside a sealed chamber under atmospheric pressure (1.013 bar) and at high ambient temperature (800 °C), which are common operating conditions for realistic SOFC [3]. The $v_{\text{in,a}}$ is set to 0.25 m s^{-1} in order to achieve almost complete fuel utilization (FU ≈ 1) at maximum current density (it is assumed that $J_{\text{max}} \approx 1$ A cm^{-2}). In the same manner, the $v_{\text{in,c}}$ is set to 2.75 m s^{-1} to achieve air utilization of about a quarter (AU ≈ 0.25), as can be seen from the results. The porosity and permeability of layers can vary from the values in Table 1, depending on specific material [3]. In this study the values are taken from our baseline model [21]. They are set to common values that are high enough to not severely limit the diffusion transport of gas species. The influences of all these parameters to final results are not studied in this paper due to excessive computational demands of the 3-D model. However, similar trends of the results should be obtained if realistic values of listed parameters were considered.

Table 1
Input parameters of baseline SOFC model.

Physical property	Symbol	Value	Unit
Reference pressure	p_{ref}	1.013	bar
Ambient temperature	T_{amb}	800	°C
Velocity of fuel at anode inlet	$v_{\text{in,a}}$	0.25	m s^{-1}
Velocity of air at cathode inlet	$v_{\text{in,c}}$	2.75	m s^{-1}
Porosity of support/active layers	ε_{p}	0.3	/
Permeability of support/active layers	κ	10^{-10}	m^2

Some modification has been done at meshing of the structure in order to speed up time-consuming transient simulations. However, reduced number of meshing points (i.e. finite elements) within the modeled structure insignificantly influences the accuracy of the final results, but significantly reduces computational time.

Fig. 1 shows meshing of the modeled SOFC structure schematically. The corresponding layers and gas chambers are also labeled. Table 2 shows dimensions and corresponding number of elements.

3.1. Moderate variation of electric load

A transient simulation of presented 3-D dynamic model was performed to obtain the response of output current density (J) to a step change of output voltage (V). The V is decreased abruptly from 0.8 V to 0.7 V at time $t = 0$ s (when steady state condition is considered) to simulate increased electric load by approximately 50%. The results of a short-period (1 s) transient analysis are obtained after each exponentially increasing time interval (starting at 1 ms). Similar experiments are presented in Ref. [19], where the voltage was decreased from 0.8 V to 0.7 V and the time-period of transient analysis was about 1 s. The main goal in the following text is to compare the response of J (V) in Fig. 2 to those presented in Ref. [19].

In Fig. 2A the current density (J) as a function of time (t) is shown for transient analysis after applying a step change of voltage (V) from 0.8 V to 0.7 V. However, the results in Fig. 2A differ from those presented in Fig. 9a–b [19], since the voltage is abruptly changed and it settles instantly in this study, whereas it settles after about 0.2 s in Ref. [19]. Due to the latter, the current has smooth transition as seen in Fig. 9b [19].

More detailed inspection reveals that current overshoots are obtained in both cases, regardless the short-time period responses of current densities differ. If the initial, maximum and final value of current density (J_{start}, J_{max} and J_{end}, all labeled in Fig. 2A) are considered, and overshoot is calculated as 100% × (J_{max}–J_{end})/J_{end}, the obtained value is about 3.4%. The obtained value of current overshoot equals 9.2% as can be seen in Table 4 in Ref. [19]. Similar overshoot (of about 9%) can also be seen in Fig. 10b in Ref. [24], but it should be noted that tubular SOFC are considered in both compared papers. The latter configuration might have some influence on the results, besides the fact that parameters of the modeled SOFC are not identical to those of tubular SOFC cells. The J at time $t = 0$ s is (almost) abruptly increased to J_{max} since the electrochemical reactions are assumed instantaneous. Due to the latter, dynamics of the current density (J) is initially very fast, as can be noticed in Fig. 2A. At time $t > 0$ s, the J exponentially decreases since the fuel and oxygen species are gradually consumed. Their supply (mass transfer of species) is restricted by inlet mass fluxes and delayed due to a distance that these species have to pass. Moreover, the supply of fuel species is also influenced by the rate of the reforming reactions.

In Fig. 2B the current density (J) as a function of time (t) is shown for transient analysis after applying an exponentially decreasing voltage (V) from 0.8 V to 0.7 V. Two time constants were considered, for slow ($T_{\text{slow}} = 50$ ms) and fast ($T_{\text{fast}} = 5$ ms) voltage transient, respectively. The first time constant (T_{slow}) was estimated from Fig. 9a in Ref. [19]. This experiment was done to show more realistic profile of J since the voltage (load) of a realistic SOFC usually varies gradually. In Fig. 2B the J_{slow} increases gradually as the V_{slow} decreases until the peak value ($J_{\text{max, slow}} = 6847$ A m^{-2}) is reached at $t = 0.4$ s. It can be noticed that the profile of J_{slow} has

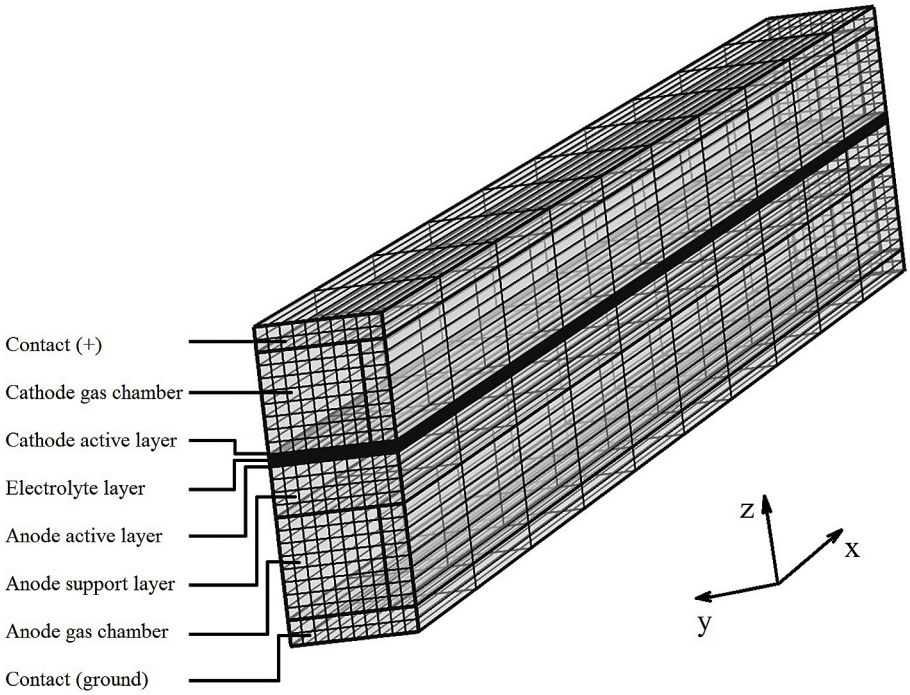

Fig. 1. Meshing of the modeled SOFC structure.

Table 2
Dimensions and meshing of the modeled SOFC structure.

Dimensions	Number of elements
Cell length (x-axis), $l = 100$ mm	10
Cathode/anode gas chamber width (y-axis), $w_{ch} = 1$ mm	8
Cathode/anode gas chamber height (z-axis), $h_{ch} = 1$ mm	8
Contact rib width (y-axis), $w_{rib} = 0.25$ mm	2
Contact rib height (z-axis), $h_{rib} = 1$ mm	8
Contact interconnect height (z-axis), $h_{ic} = 0.25$ mm	2
Cathode active layer thickness (z-axis), $d_c = 50$ μm	5
Electrolyte layer thickness (z-axis), $d_e = 10$ μm	2
Anode active layer thickness (z-axis), $d_a = 50$ μm	5
Anode support layer thickness (z-axis), $d_s = 0.5$ mm	4

similar shape as the profile of current I in Fig. 9a in Ref. [19] if relative changes in J_{slow} and I are compared (+49.7% vs. 43.1%).

However, relative overshoot (+0.5%) is much smaller if compared to that in Table 4 in Ref. [19]. Similar observation can be made for J_{fast}, which increases faster than J_{slow} before it reaches its peak value ($J_{max,\,fast} = 6890$ A m^{-2}) at $t = 0.025$ s. Relative overshoot (+1.2%) is also smaller than the overshoot in Table 4 in Ref. [19].

In Fig. 3A the fuel utilization (FU) and air utilization (AU) as a function of time (t) after applying a step change of voltage (V) from 0.8 V to 0.7 V is shown. It can be noticed that dynamics of FU and AU are quite different. The FU needs about 1 s, whereas the AU needs only about 0.05 s to reach its steady-state value. This can be explained by taking into consideration that porous anode support layer is quite thick (0.5 mm) and it contains a considerable amount of fuel.

The consumption of fuel species is increased during the transient and it influences the local concentrations (partial pressures) of fuel gas species within the porous anode support/active layer. Consequently, the rate of producing fuel species by reforming and water-gas-shift (WGS) reactions varies with time. It takes a period of time that steady-state concentrations of fuel species are established within the porous anode support/active layer. This is reflected in slowly varying FU, which is calculated by the following equation [33]:

$$FU = 1 - \frac{4\cdot\dot{n}_{CH_4,out} + \dot{n}_{H_2,out} + \dot{n}_{CO,out}}{4\cdot\dot{n}_{CH_4,in} + \dot{n}_{H_2,in} + \dot{n}_{CO,in}}, \tag{15}$$

where the $\dot{n}_{CH4,in/out}$, $\dot{n}_{H2,in/out}$, and $\dot{n}_{CO,in/out}$ is the total inlet/outlet mole flux (in mol s^{-1}) of methane (CH_4), hydrogen (H_2) nad carbon monoxide (CO) gas specie at the fuel (anode) inlet/outlet side, respectively.

In contrast, the porous cathode layer is very thin (50 μm) and it contains a small amount of air species. It takes a short period of time that steady-state concentrations of air species are established within the porous cathode active layer. Due to the latter, AU varies faster than FU does, and it is calculated by the following equation:

$$AU = 1 - \frac{\dot{n}_{O_2,out}}{\dot{n}_{O_2,in}}, \tag{16}$$

where the $\dot{n}_{O2,in/out}$ is the total inlet/outlet mole flux (in mol s^{-1}) of oxygen (O_2) gas specie at the air (cathode) inlet/outlet side.

In Fig. 3B the fuel utilization (FU) and air utilization (AU) as a

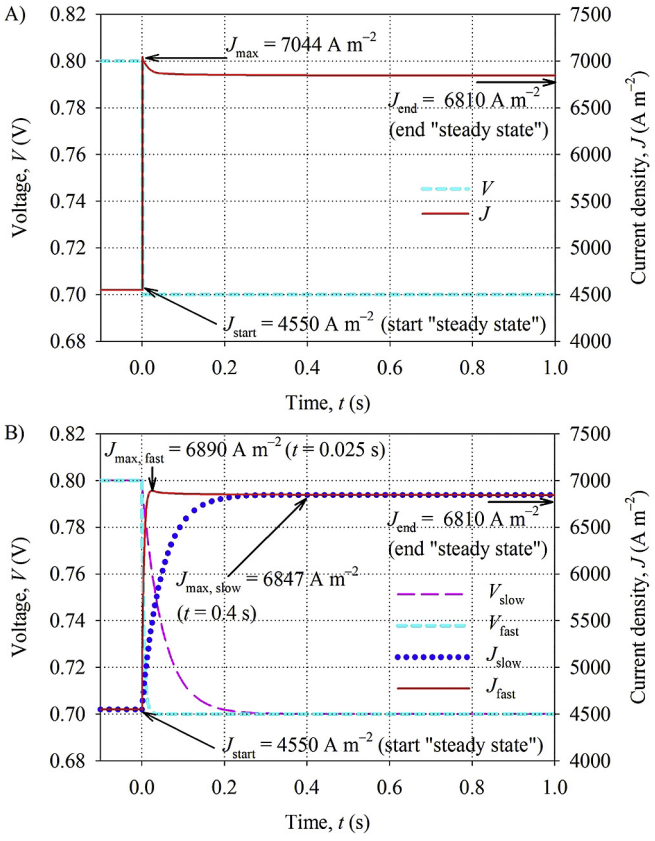

Fig. 2. The current density (J) as a function of time (t) after A) a step change of voltage (V) from 0.8 V to 0.7 V, and B) an exponentially decreasing voltage (V) from 0.8 V to 0.7 V. Time constant of variable V is 50 ms (slow) or 5 ms (fast).

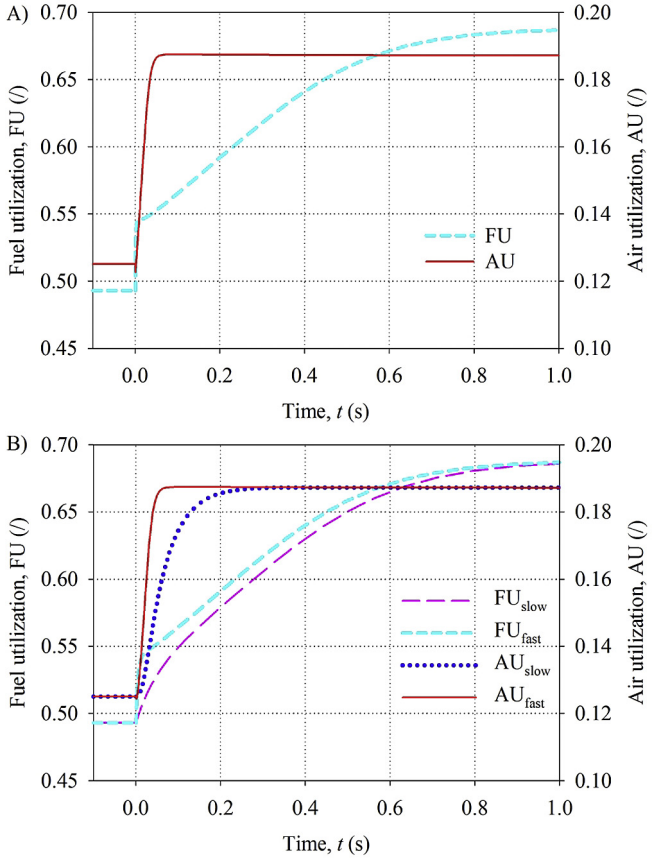

Fig. 3. Fuel utilization (FU) and air utilization (AU) as a function of time (t) after A) a step change of voltage and B) an exponentially decreasing voltage from 0.8 V to 0.7 V.

function of time (t) after applying an exponentially decreasing voltage (V) from 0.8 V to 0.7 V is shown. The dynamics of all quantities are slower compared to those in Fig. 3A, especially of FU_{slow} and AU_{slow}. The latter can be understood since the J_{slow} increases at slower rate than the J_{fast} in Fig. 2B or the J in Fig. 2A does. It is also important to note that the profile of AU_{slow} is almost proportional to the profile of J_{slow}, whereas the profile of FU_{slow} differs from J_{slow}.

This difference could be attributed to thicker porous anode support layer and reforming/WGS reactions, as discussed previously.

From these simulation results it can concluded that the current density (J) overshoots have no evident influence on fuel utilization (FU) by means of causing local fuel starvation. The maximum value of FU is about 0.7, which is far from fuel starvation since the results also indicate that minimum mass fractions of fuel species are still high within the porous anode active layer. The problem of local fuel starvation is addressed in Section 3.2 where large variations of electric load are considered.

In Fig. 4 the SOFC output voltage (V) as a function of time (t) is shown for transient analysis after applying a current density (J) step change from 4550 A m^{-2} to 6810 A m^{-2}. The J is increased by approximately 50% at $t = 0$ s, and consequently, due to internal resistance of the SOFC structure (electrolyte and electrodes have finite electrical conductivity) an instantaneous voltage drop (ΔV) of about 91 mV can be noticed. At $t > 0$ s the voltage (V) decreases since the species are consumed, as explained before, and concentration overpotential increases. No voltage (or current density) overshoot can be noticed in this case. Please note that the applied

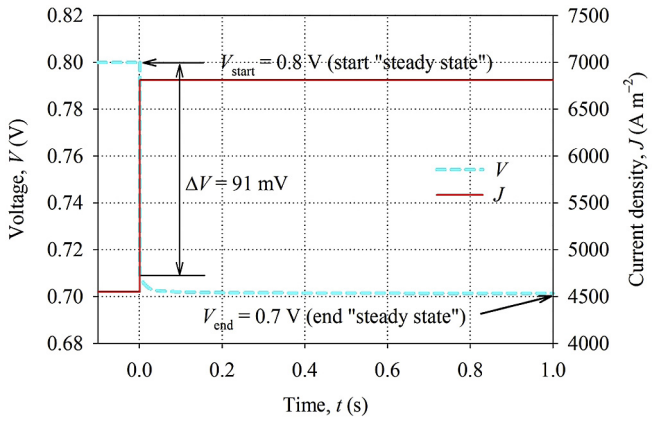

Fig. 4. Output voltage (V) as a function of time (t) after a step change of current density (J) from 4550 A m^{-2} to 6810 A m^{-2} at $t = 0$ s.

step change in J (Fig. 4) is equal to the difference between J_{end} and J_{start} (Fig. 2A). Similarly, the applied step change in V (Fig. 2A) is equal to the difference between V_{end} and V_{start} (Fig. 4). To compare, no short-period voltage overshoot can be noticed in Fig. 10a in Ref. [24], while the voltage drop is about 25 mV lower ($\Delta V \approx 66$ mV) in that case.

From these observations it can be concluded that load variations should be limited to prevent current overshoots, which can possibly lead to local fuel starvation, and consequently, degradation of realistic SOFC. Another possibility is limiting the rate of voltage

change, which can be realized by filtering of the voltage reference for electronic load with low-pass filter having appropriate time constant. The time constant $T_{slow} = 50$ ms for applied voltage (V) considerably reduced current density (J) overshoot, as seen in Fig. 2B.

3.2. Large variation of electric load

A detailed study of a case where large load variations are present is done in the following. This study shows operational conditions that can possibly cause degradation of a realistic SOFC. Four diverse thicknesses of the porous anode support layer (d_s) are considered, i.e. 0.1 mm, 0.2 mm, 0.5 mm and 1.0 mm, to find whether the reforming/WGS reactions and stored fuel species within the layer can mitigate the effect of local fuel starvation. However, a thickness below 0.1 mm or above 1.0 mm is very unlike for practical implementation, so it is not considered in this study. It should be mentioned that the other dimensions (Table 2) of the modeled fuel cell can also be varied, but they do not influence the fuel starvation directly, since the fuel gas is mainly contained and reformed within the porous anode support layer. Moreover, the support layer represents the largest part of the fuel cell structure (excluding the contacts and interconnects), as can be seen from thicknesses of layers in Table 2, and from this point of view, it is of high importance to optimize the consumption of material in realistic devices.

Fig. 5 shows the current density (J) of modeled SOFC after a step change of voltage (V) from 0.8 V to 0.6 V at time $t = 0$ s. Similar experiment has been performed in Ref. [34], but only an array of 8×8 (64) 1-D unit cells is used to model a realistic co-, counter-, and cross-flow SOFC when large load variations (i.e. voltage is abruptly decreased from 0.96 V to 0.84 V or 0.7 V) are considered. The J in this case is increased by approximately 100% (by a factor of about 3.75 or 6.6 in Ref. [34]), considering its start (J_{start}) and its end value (J_{end}), for each of the selected structures, i.e. SOFC with $d_s = 0.1$ mm, 0.2 mm, 0.5 mm and 1.0 mm, respectively. Detailed values of start (J_{start}), maximum (J_{max}), end (J_{end}), relative increment (ΔJ) and overshoot of J are shown in Table 3. Regardless the time constant of the J in this case is much shorter than that in Ref. [34], similar overshoots of J can be observed. However, the pending question is if the thickness of the anode support layer in combination with spatially dependent concentration of fuel gas within the support layer can be considered properly with 1-D model. The latter is cleared by comparing the concentrations of fuel gas species at the end of this section.

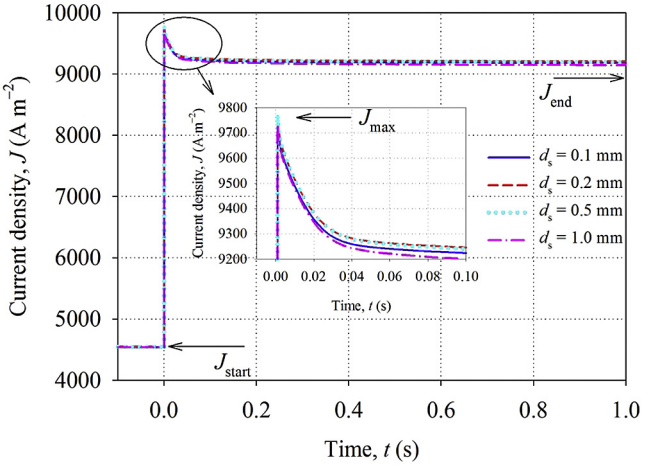

Fig. 5. The current density (J) of modeled SOFC as a function of time (t) after a step change of voltage (V) from 0.8 V to 0.6 V at $t = 0$ s.

Table 3
Values of start (J_{start}), maximum (J_{max}), end (J_{end}), relative increment (ΔJ) and overshoot of current density at diverse thickness of porous anode support layer (d_s).

d_s (mm)	J_{start} (A m^{-2})	J_{max} (A m^{-2})	J_{end} (A m^{-2})	ΔJ (%)	Overshoot (%)
0.1	4537	9734	9091	100.4	7.1
0.2	4549	9762	9109	100.2	7.2
0.5	4550	9762	9095	99.9	7.3
1.0	4534	9723	9040	99.4	7.6

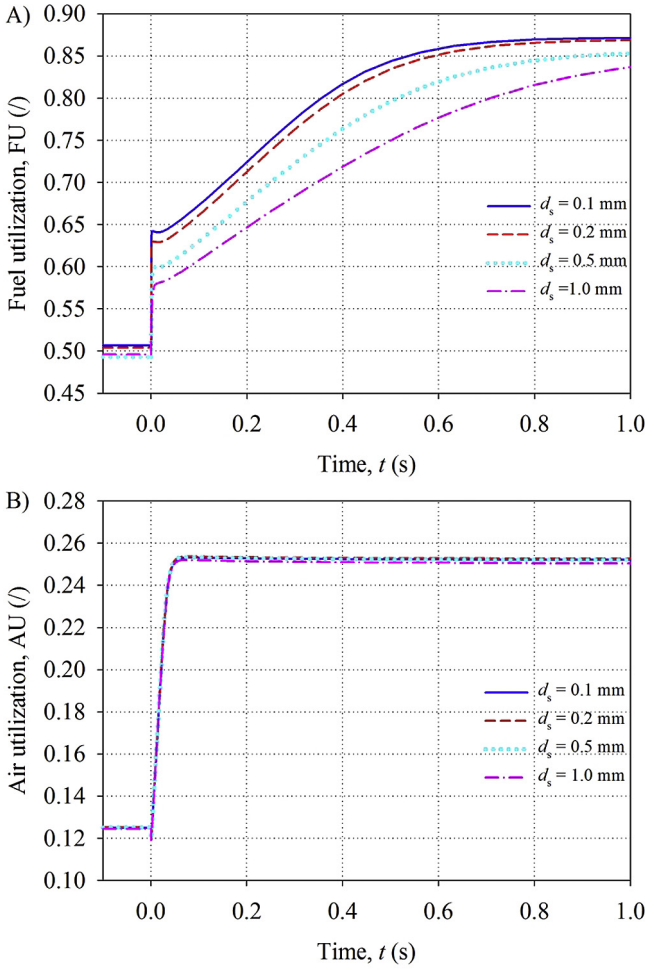

Fig. 6. The fuel (FU) and air utilization (AU) of modeled SOFC as a function of time (t) after a step change of voltage (V) from 0.8 V to 0.6 V at $t = 0$ s.

Table 4
Values of start (FU_{start}), maximum (FU_{max}), end fuel utilization (FU_{end}), and time delay (t_d) of FU_{max} occurence after a step change of voltage (V) from 0.8 V to 0.6 V (at time $t = 0$ s) at diverse thickness of porous anode support layer (d_s).

d_s (mm)	FU_{start} (/)	FU_{max} (/)	FU_{end} (/)	t_d (s)
0.1	0.507	0.872	0.866	1.26
0.2	0.504	0.869	0.864	1.26
0.5	0.493	0.857	0.852	1.58
1.0	0.496	0.855	0.851	2.24

The J_{start}, J_{max}, and J_{end} are slightly increased by increasing the thickness of porous anode support layer if $d_s < 0.2$ mm. A thicker (proportionally with d_s) porous anode support layer produces more fuel species (hydrogen and carbon monoxide) by methane

reforming since more reaction sites are present within the layer due to larger volume. Higher local concentration (mass fraction) of fuel species slightly lowers the concentration overpotentials, and consequently, higher current density is generated.

However, the J_{start}, J_{max} and J_{end}, are decreased if $d_s > 0.5$ mm since the voltage drop on porous anode support layer is higher than the reduction of concentration overpotentials. The relative increment (ΔJ) and overshoot of current density are also varied with d_s, but the variations are negligible.

Fig. 6 shows the fuel (FU) and air utilization (AU) after a step change of voltage (V) from 0.8 V to 0.6 V at time $t = 0$ s. The maximum fuel utilization (FU_{max}) is reached in 1.26 s, 1.26 s, 1.58 s and 2.24 s if the thickness of porous anode support layer (d_s) equals 0.1 mm, 0.2 mm, 0.5 mm and 1.0 mm, respectively, as shown in Table 4. It can also be noticed that FU_{end} (FU_{max}) decreases with increasing the d_s. Please note that J_{end} (J_{max}) also decreases when $d_s > 0.2$ mm (0.5 mm). However, the $d_s > 0.5$ mm has a little effect on decreasing the FU_{end} (FU_{max}). The dynamics of FU is also slower if d_s increases, which indicates the effect of producing of fuel species (with reforming and WGS reactions) within the porous anode support layer, as discussed before. The maximum air utilization (AU_{max}) is reached in 0.08 s, 0.08 s, 0.08 s and 0.07 s if the thickness of porous anode support layer (d_s) equals 0.1 mm, 0.2 mm, 0.5 mm and 1.0 mm, respectively, as shown in Table 5. It can also be noticed that AU_{end} (AU_{max}) decreases with increasing the d_s above 0.2 mm. The latter is attributed to reduced current density if $d_s > 0.2$ mm, as can be seen in Fig. 5. It is important to note that inlet air flow rate must be sufficiently high to prevent overpotential losses, which occur when the concentration of oxygen within the porous cathode active layer is low. In this case, just about one quarter of oxygen is used when maximum air utilization ($AU_{max} \approx 0.25$) occurs.

The results in Table 4 indicate that a thicker porous anode support layer mitigates the local fuel starvation since lower FU is accomplished when the d_s is higher. These observations are confirmed by analysing the minimum mass fractions of fuel species within the porous anode active layer, as shown in Fig. 7. It can be noticed that the minimum mass fraction of carbon monoxide (Y_{CO}, Fig. 7A) and hydrogen (Y_{H2}, Fig. 7B) drop after a step change of voltage from 0.8 V to 0.6 V at time $t = 0$ s. Moreover, if the thickness of the porous anode support layer is small (e.g. $d_s = 0.1$ mm), the Y_{CO} and Y_{H2} drop to critical low values, as seen in Tables 6 and 7, which can possibly lead to local fuel starvation within the porous anode active layer. Besides this, a considerable undershoot of each minimum mass fraction can be observed, too. The latter indicates that SOFC with a thin porous anode support layer is potentially prone to local fuel starvation and, consequently, degradation of the porous anode electrode. However, this deteriorating effect can be prevented or, at least, mitigated by increasing the thickness of porous anode support layer (d_s), increasing (decreasing) the flow rate of fuel (fuel utilization), or limiting maximum current density of a realistic SOFC. As can be seen from the simulation results in Fig. 7A and B, the thickness of porous anode support layer (d_s) should be around 0.5 mm to mitigate local fuel starvation within the porous anode active layer.

Table 5
Values of start (AU_{start}), maximum (AU_{max}), end air utilization (AU_{end}), and time delay (t_d) of AU_{max} occurence after a step change of voltage (V) from 0.8 V to 0.6 V (at time $t = 0$ s) at diverse thickness of porous anode support layer (d_s).

d_s (mm)	AU_{start} (/)	AU_{max} (/)	AU_{end} (/)	t_d (s)
0.1	0.125	0.253	0.249	0.08
0.2	0.125	0.254	0.250	0.08
0.5	0.125	0.253	0.249	0.08
1.0	0.124	0.252	0.247	0.07

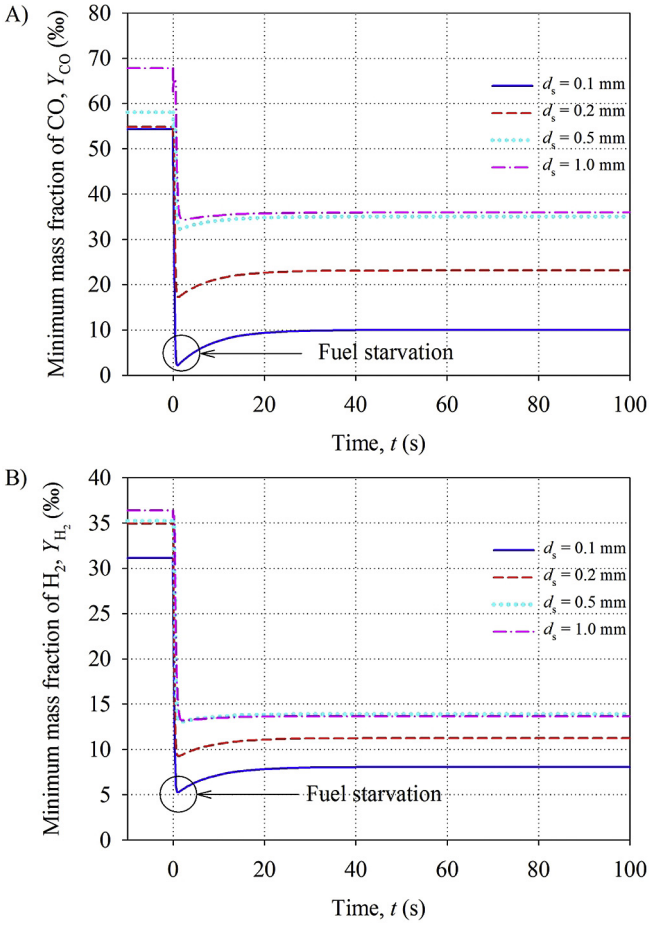

Fig. 7. Minimum mass fraction of carbon monoxide (Y_{CO}) and hydrogen (Y_{H2}) within the porous anode active layer after a step change of voltage from 0.8 V to 0.6 V (at time $t = 0$ s).

Table 6
Minimum values of start ($Y_{CO,start}$), minimum ($Y_{CO,min}$), end mass fraction of carbon monoxide ($Y_{CO,end}$) within the porous anode active layer, and time delay (t_d) of $Y_{CO,min}$ occurence after a step change of voltage from 0.8 V to 0.6 V (at time $t = 0$ s) at diverse thickness of porous anode support layer (d_s).

d_s (mm)	$Y_{CO,start}$ (‰)	$Y_{CO,min}$ (‰)	$Y_{CO,end}$ (‰)	t_d (s)
0.1	54.33	2.17	10.00	1.00
0.2	54.84	17.23	23.14	1.12
0.5	58.09	32.33	35.02	1.58
1.0	67.80	34.32	35.91	2.24

Table 7
Minimum values of start ($Y_{H2,start}$), minimum ($Y_{H2,min}$), end mass fraction of hydrogen ($Y_{H2,end}$) within the porous anode active layer, and time delay (t_d) of $Y_{H2,min}$ occurence after a step change of voltage from 0.8 V to 0.6 V (at time $t = 0$ s) at diverse thickness of porous anode support layer (d_s).

d_s (mm)	$Y_{H2,start}$ (‰)	$Y_{H2,min}$ (‰)	$Y_{H2,end}$ (‰)	t_d (s)
0.1	31.12	5.25	8.05	1.00
0.2	34.95	9.23	11.24	1.12
0.5	35.23	13.04	13.90	1.58
1.0	36.38	13.19	13.66	2.24

An important advantage of 3-D dynamic model is deep insight into local concentrations (mass fractions) of fuel species that cannot be measured in realistic SOFC. The results of simulations also give

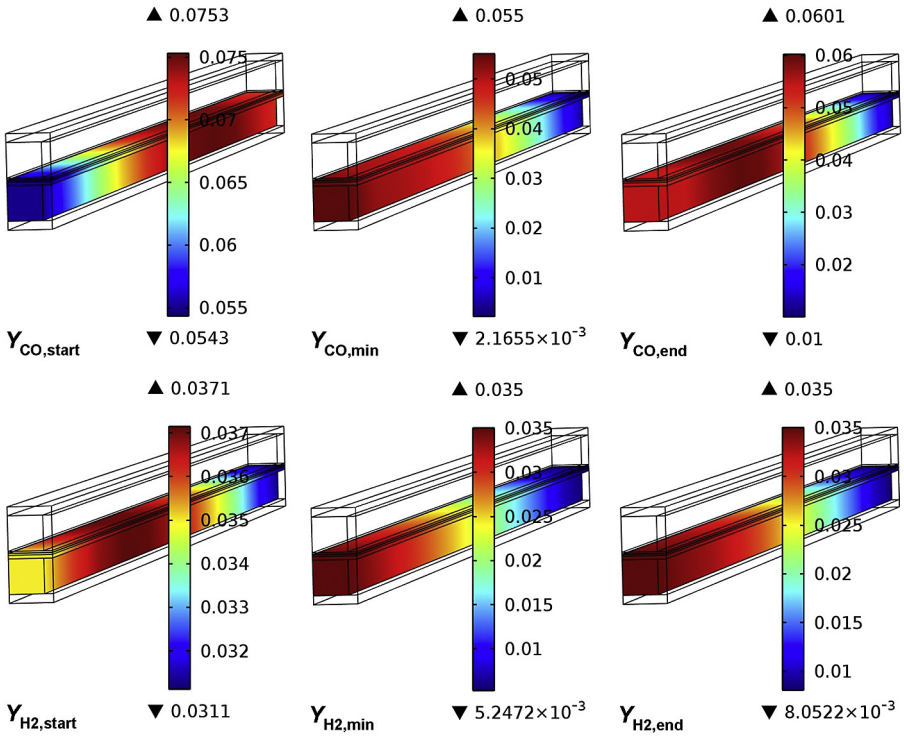

Fig. 8. 3-D profiles of mass fractions of fuel species ($Y_{CO/H2,start}$, $Y_{CO/H2,min}$ and $Y_{CO/H2,end}$) within the porous anode active/support layer and anode gas chamber at time $t = 0$ s, 1 s, and 200 s, respectively, after the step change of applied voltage from 0.8 V to 0.6 V at $t = 0$ s.

some guidelines for setting appropriate FU, which has to be below a specified value (about 0.85 in this case, as seen in Table 4) to prevent local fuel starvation during large load variations. Moreover, 3-D model is also superior to 0-D, 1-D or 2-D models, since these cannot handle the anode support layer thickness and spatially dependent concentrations of fuel gas properly. For example, Fig. 15 and 16 in Ref. [34] show concentrations of fuel gas (hydrogen) as 2-D contour plots, obtained by using the model of 8 × 8 (64) 1-D unit cells in cross-flow configuration. As it becomes evident, no thickness dependent fuel gas concentration can be resolved. The latter might become important since a thick support layer or low porosity/permeability of the layer can limit the transport of fuel gas species. In contrast, 3-D model generates a complete spatial distribution of fuel gas concentrations (mass fractions), as shown in Fig. 8, and it has a considerable advantage over the 0-D, 1-D or 2-D models.

Fig. 8 illustrates the 3-D profiles of mass fractions of fuel species (Y_{CO} and Y_{H2}) within the porous anode active/support layer (and anode gas chamber) at time $t = 0$ s, 1 s, and 200 s after the step change of voltage from 0.8 V to 0.6 V at $t = 0$ s (the structure of SOFC with $d_s = 0.1$ mm is considered) to show situation when the minimum $Y_{CO/H2,start}$, $Y_{CO/H2,min}$ and $Y_{CO/H2,end}$ are obtained, respectively.

As can be seen from these plots, the minimum values of $Y_{H2,start}$, $Y_{CO/H2,min}$ and $Y_{CO/H2,end}$ emerge at the fuel outlet, whereas the minimum (maximum) value of $Y_{CO,start}$ emerges at the fuel inlet (close to the outlet). The latter is due to reforming reactions that produce carbon monoxide within the porous anode support layer. The result of reforming is that the $Y_{CO,start}$ at the fuel outlet is higher than $Y_{CO,start}$ at the fuel inlet. However, this situation is reversed when the current density (J) is increased (for $t > 0$ s, as can be seen in Fig. 5) since more carbon monoxide is consumed by electrochemical reactions to generate higher J. Due to the latter, the $Y_{CO,min/end}$ at the fuel inlet is higher than $Y_{CO,min/end}$ at the fuel outlet.

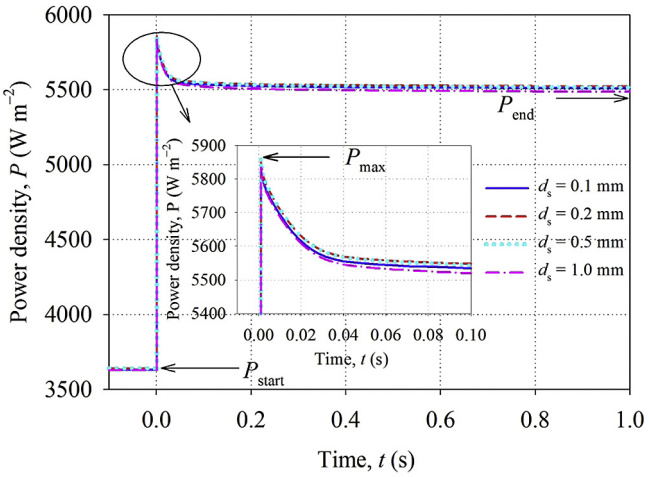

Fig. 9. The power density (P) of the modeled SOFC as a function of time (t) after a step change of voltage (V) from 0.8 V to 0.6 V (at $t = 0$ s).

A detailed inspection also reveals that the highest $Y_{H2,start}$ occurs around the middle length of porous anode support layer due to the reforming reactions. When the current density (J) is increased, more hydrogen is consumed, and the highest $Y_{H2,min/end}$ emerges at the fuel inlet.

The presented results confirm that 3-D modeling and transient analysis of SOFC give us valuable data about quantities that are time and spatially dependent. The analysis of local mass fractions of fuel species indicates local fuel starvation within porous anode active layer during the load variations, which can possibly accelerate degradation rate of a realistic SOFC.

Table 8
Values of start (P_{start}), maximum (P_{max}), end (P_{end}), relative increment (ΔP) and overshoot of power density (P) at diverse thickness of porous anode support layer (d_s).

d_s (mm)	P_{start} (W m^{-2})	P_{max} (W m^{-2})	P_{end} (W m^{-2})	ΔP (%)	Overshoot (%)
0.1	3630	5841	5454	50.2	7.1
0.2	3639	5857	5466	50.2	7.2
0.5	3640	5857	5457	49.9	7.3
1.0	3627	5834	5424	49.5	7.6

3.3. Power density and electrical efficiency at large variations of electric load

The power density (P) and electrical conversion efficiency (η) of the modeled SOFC are studied by considering variable operating conditions, since dynamic profiles of P and η can significantly differ from their steady-state profiles. Due to a small amount of such results presented to date, the transient analysis of P and η after applied large load variation (as already shown in Section 3.2) is done in this section. Fig. 9 shows power density (P) of the modeled SOFC after a step change of voltage from 0.8 V to 0.6 V ($t = 0$ s).

The profile of P in Fig. 9 has similar shape as the profile of J in Fig. 5, since the power density (P) is calculated as a product of current density (J) and voltage (V) of the SOFC. Detailed values of start (P_{start}), maximum (P_{max}), end (P_{end}), relative increment (ΔP) and overshoot of power density (P) are shown in Table 8. Please note that the values are also dependent on the thickness of porous anode support layer (d_s).

It is important to note that maximum values of P_{start}, P_{max}, and P_{end} occur at $d_s = 0.2$–0.5 mm, which indicates the most appropriate thickness of the porous anode support layer by means of achieving high output power of the SOFC. The relative increment of power density (ΔP) is about 50%, which is about a half of relative increment of current density (ΔJ), as can be seen in Table 3. The overshoots in Table 8 are identical to those in Table 3.

Finally, the electrical conversion efficiency (η) is analyzed. The η could be calculated in different ways. A common approach is to evaluate the ratio between output (P_{out}) and input power (P_{in}). In this study, the following equation was used to obtain the η of the modeled SOFC [29]:

$$\eta = \frac{P_{out}}{P_{in}} = \frac{V \cdot J \cdot A}{\dot{n}_{CH_4,in} \cdot LHV_{CH_4} + \dot{n}_{H_2,in} \cdot LHV_{H_2} + \dot{n}_{CO,in} \cdot LHV_{CO}}, \quad (17)$$

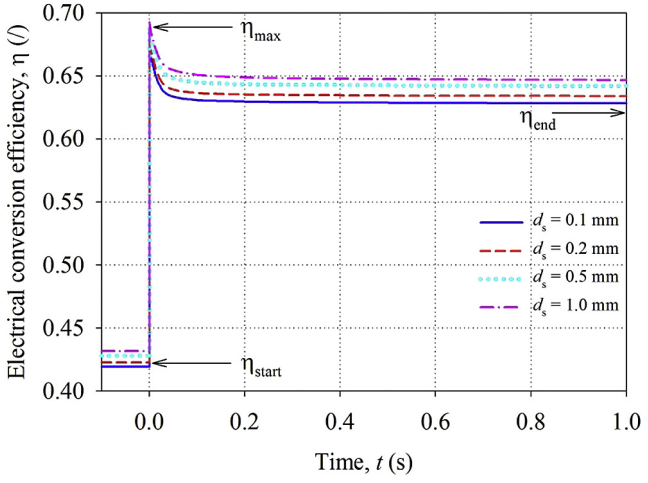

Fig. 10. The electrical conversion efficiency (η) as a function of time (t) after a step change of voltage from 0.8 V to 0.6 V at $t = 0$ s.

Table 9
Values of start (η_{start}), maximum (η_{max}), end (η_{end}), relative increment ($\Delta\eta$) and overshoot of conversion efficiency (η) at diverse thickness of porous anode support layer (d_s).

d_s (mm)	η_{start} (/)	η_{max} (/)	η_{end} (/)	$\Delta\eta$ (%)	Overshoot (%)
0.1	0.419	0.674	0.623	48.7	8.2
0.2	0.423	0.680	0.629	48.7	8.1
0.5	0.428	0.689	0.637	48.8	8.2
1.0	0.432	0.694	0.642	48.6	8.1

where V is voltage, J is current density, A is contacted area of the SOFC, $\dot{n}_{CH4,in}$, $\dot{n}_{H2,in}$, and $\dot{n}_{CO,in}$ is inlet mole flux (in mol s^{-1}) of methane (CH_4), hydrogen (H_2) nad carbon monoxide (CO), whereas LHV_{CH4} = 800 kJ mol^{-1}, LHV_{H2} = 241 kJ mol^{-1} and LHV_{CO} = 283 kJ mol^{-1} is lower heat value of the corresponding fuel specie.

Fig. 10 shows the electrical conversion efficiency (η) as a function of time (t) after a step change of voltage from 0.8 V to 0.6 V at $t = 0$ s. The η is increased after the applied load variation (current density J is increased, as can be seen in Fig. 5) since higher amount of supplied fuel is efficiently used by electrochemical reactions. However, the overpotential and ohmic losses are increased (higher voltage drop on SOFC structure) due to higher J, so the η is increased by about 50% only (similar to relative increment of power density P, as can be seen in Table 8). Detailed values of start (η_{start}), maximum (η_{max}), end (η_{end}), relative increment ($\Delta\eta$) and overshoot of electrical conversion efficiency (η) are shown in Table 9.

It can be noticed that η increases with increasing the thickness of porous anode support layer (d_s). The η_{end} (η_{max}) of SOFC with $d_s = 1.0$ mm is about 0.02 higher than the η_{end} (η_{max}) of SOFC with $d_s = 0.1$ mm. The latter becomes quite important issue when high operating power of a realistic SOFC is needed. However, the results also indicate (not shown in Table 9) that increasing the d_s above 1.0 mm has insignificant influence on η_{end} (η_{max}). In contrast, the η_{end} of a SOFC with $d_s = 2.5$ mm is even lower than η_{end} of a SOFC with $d_s = 1.0$ mm, so $d_s = 1.0$ mm seems to be appropriate thickness of porous anode support layer in terms of achieving high η.

The simulation results show that the thickness of porous anode support layer (d_s) is one of key parameters to improve electrical conversion efficiency (η). However, there is obviously a trade-off between actual improvement of η and consumption of precious materials, e.g. nickel/yttria stabilized zirconia (Ni/YSZ) for producing porous anode support layer, but such optimization is beyond the scope of the presented paper.

It can be concluded that this study delivers many important insights into operation of SOFC and represents a considerable progress in transient analysis of SOFC's responses since 3-D dynamic model is addressed, which has some crucial advantages over the simplified 0-D, 1-D or 2-D models.

4. Conclusion

The modeling of a single, planar, anode supported, solid oxide fuel cell (SOFC) was presented in this paper. Dynamic model was built in three dimensions (3D) in COMSOL Multiphysics® 4.3. The

current density (J), fuel utilization (FU) and air utilization (AU) of SOFC were analyzed when the electric load was abruptly increased by approximately 50%. The results were compared with those from literature. Similar trends in J profiles were observed if relative variation of current density (ΔJ) was considered. Overshoots of J were also observed, but these were smaller than those presented in other studies.

Furthermore, four diverse thicknesses of porous anode support layer ($d_s = 0.1$ mm, 0.2 mm, 0.5 mm and 1.0 mm, respectively) were studied by means of transient response of the modeled SOFC to load variations by approximately 100%. The simulation results showed that the SOFC with thin porous anode support layer ($d_s = 0.1$ mm) is prone to local fuel starvation during load variations since local concentrations of fuel species within the porous anode active layer approach to zero. The d_s was found important parameter of SOFC by means of mitigating the local fuel starvation. The FU could be an indicator of fuel starvation, but its measurement cannot give deep insight into local fuel species concentrations, so the three-dimensional (3-D) dynamic model is inevitable tool to obtain more detailed insight. The FU above 0.85 could be potentially dangerous for fuel starvation, and consequently, degradation of a realistic SOFC. The limitation of J or increased (decreased) inlet flow rate of fuel (FU) would prevent fuel starvation.

The power density (P) and electrical conversion efficiency (η) of the modeled SOFC were also studied. The simulation results indicated that the P slightly decreases, but the η increases with increasing the d_s. The η of SOFC with $d_s = 1.0$ mm is about 0.02 higher than the η of SOFC with $d_s = 0.1$ mm. This becomes quite important issue when high operating power of a realistic SOFC is needed.

More experimental work should be performed to verify the simulation results. Unfortunately, the experiments are very expensive and time consuming. Currently, we cannot afford such tests, so the paper lacks a complete verification. However, the simulation results showed the problem of local fuel starvation during the load variations and the effect of d_s on η. The results also gave some guidelines to help experimentalists how to mitigate the degradation process and to improve the η by appropriate design and control of a realistic SOFC.

Acknowledgment

The author would like to acknowledge the support of the Slovenian Research Agency through Research Programme P2-0001.

References

[1] Costamagna P, Selimovic A, Del Borghi M, Agnew G. Electrochemical model of the integrated planar solid oxide fuel cell (IP-SOFC). Chem Eng J 2004;102:61–9.
[2] Janardhanan VM, Deutschmann O. Modeling of solid-oxide fuel cells. Z Phys Chem 2007;221:443–78.
[3] Kakaç S, Pramuanjaroenkij A, Zhou XY. A review of numerical modeling of solid oxide fuel cells. Int J Hydrogen Energy 2007;32:761–86.
[4] Haga K, Adachi S, Shiratori Y, Itoh K, Sasaki K. Poisoning of SOFC anodes by various fuel impurities. Solid State Ionics 2008;179:1427–31.
[5] Holzer L, Iwanschitz B, Hocker T, Münch B, Prestat M, Wiedenmann D, et al. Microstructure degradation of cermet anodes for solid oxide fuel cells: quantification of nickel grain growth in dry and in humid atmospheres. J Power Sources 2011;196:1279–94.
[6] Tu H, Stimming U. Advances, aging mechanisms and lifetime in solid-oxide fuel cells. J Power Sources 2004;127:284–93.
[7] Larrain D, Van herle J, Favrat D. Simulation of SOFC stack and repeat elements including interconnect degradation and anode reoxidation risk. J Power Sources 2006;161:392–403.
[8] Das T, Narayanan S, Mukherjee R. Steady-state and transient analysis of a steam-reformer based solid oxide fuel cell system. J Fuel Cell Sci Technol 2010;7. 011022–1.
[9] Lin C-K, Liu Y-A, Wu S-H, Liu C-K, Lee R-Y. Joint strength of a solid oxide fuel cell glass-ceramic sealant with metallic interconnect in a reducing environment. J Power Sources 2015;280:272–88.
[10] Robinson JB, Brown LD, Jervis R, Taiwo OO, Heenan TMM, Millichamp J, et al. Investigating the effect of thermal gradients on stress in solid oxide fuel cell anodes using combined synchrotron radiation and thermal imaging. J Power Sources 2015;288:473–81.
[11] Yokokawa H, Yamaji K, Brito ME, Kishimoto H, Horita T. General considerations on degradation of Solid Oxide Fuel Cell anodes and cathodes due to impurities in gases. J Power Sources 2011;196:7070–5.
[12] Ryan EM, Xu W, Sun X, Khaleel MA. A damage model for degradation in the electrodes of solid oxide fuel cells: modeling the effects of sulfur and antimony in the anode. J Power Sources 2012;210:233–42.
[13] Waldbillig D, Wood A, Ivey DG. Thermal analysis of the cyclic reduction and oxidation behaviour of SOFC anodes. Solid State Ionics 2005;176:847–59.
[14] Madani O, Das T. Feedforward based transient control in solid oxide fuel cells. Control Eng Pract 2016;56:86–91.
[15] Thounthong P, Raël S, Davat B. Control strategy of fuel cell/supercapacitors hybrid power sources for electric vehicle. J Power Sources 2006;158:806–14.
[16] Allag T, Das T. Robust control of solid oxide fuel cell ultracapacitor hybrid system. IEEE Trans Control Syst Technol 2012;20(No. 1):1–10.
[17] Kazempoor P, Ommi F, Dorer V. Response of a planar solid oxide fuel cell to step load and inlet flow temperature changes. J Power Sources 2011;196:8948–54.
[18] Chaisantikulwat A, Diaz-Goano C, Meadows ES. Dynamic modelling and control of planar anode-supported solid oxide fuel cell. Comput Chem Eng 2008;32:2365–81.
[19] Bhattacharyya D, Rengaswamy R, Finnerty C. Dynamic modeling and validation studies of a tubular solid oxide fuel cell. Chem Eng Sci 2009;64:2158–72.
[20] Albrecht KJ, Braun RJ. The effect of coupled mass transport and internal reforming on modeling of solid oxide fuel cells part II: benchmarking transient response and dynamic model fidelity assessment. J Power Sources 2016;304:402–8.
[21] Nerat M, Juričić Đ. A comprehensive 3-D modeling of a single planar solid oxide fuel cell. Int J Hydrogen Energy 2016;41:3613–27.
[22] Sedghisigarchi K, Feliachi A. Dynamic and transient analysis of power distribution systems with fuel cells—part II: control and stability enhancement. IEEE Trans Energy Convers 2004;19(No. 2):429–34.
[23] Iora P, Aguiar P, Adjiman CS, Brandon NP. Comparison of two IT DIR-SOFC models: impact of variable thermodynamic, physical, and flowproperties. Steady-state and dynamic analysis. Chem Eng Sci 2005;60:2963–75.
[24] Qi Y, Huang B, Luo J. Dynamic modeling of a finite volume of solid oxide fuel cell: the effect of transport dynamics. Chem Eng Sci 2006;61:6057–76.
[25] Duhn JD, Jensen AD, Wedel S, Wix C. Optimization of a new flow design for solid oxide cells using computational fluid dynamics modelling. J Power Sources 2016;336:261–71.
[26] Xu H, Chen B, Liu J, Ni M. Modeling of direct carbon solid oxide fuel cell for CO and electricity cogeneration. Appl Energy 2016;178:353–62.
[27] Zhang Z, Yue D, Yang G, Chen J, Zheng Y, Miao H, et al. Three-dimensional CFD modeling of transport phenomena in multi-channel anode-supported planar SOFCs. Int J Heat Mass Transf 2015;84:942–54.
[28] Barelli L, Bidini G, Ottaviano A. Solid oxide fuel cell modelling: electrochemical performance and thermal management during load-following operation. Energy 2016;115:107–19.
[29] Luo XJ, Fong KF. Development of 2D dynamic model for hydrogen-fed and methane-fed solid oxide fuel cells. J Power Sources 2016;328:91–104.
[30] Amedi HR, Bazooyar B, Pishvaie MR. Control of anode supported SOFCs (solid oxide fuel cells): Part I. mathematical modeling and state estimation within one cell. Energy 2015;90:605–21.
[31] Lee S, Kim H, Yoon KJ, Son J-W, Lee J-H, Kim B-K, et al. The effect of fuel utilization on heat and mass transfer within solid oxide fuel cells examined by three-dimensional numerical simulations. Int J Heat Mass Transf 2016;97:77–93.
[32] Ho TX. Dynamic characteristics of a solid oxide fuel cell with direct internal reforming of methane. Energy Convers Manag 2016;113:44–51.
[33] Chen S, Lior N, Xiang W. Coal gasification integration with solid oxide fuel cell and chemical looping combustion for high-efficiency power generation with inherent CO_2 capture. Appl Energy 2015;146:298–312.
[34] Gemmen RS, Johnson CD. Effect of load transients on SOFC operation–current reversal on loss of load. J Power Sources 2005;144:152–64.